Final Report

Title: Fundamental studies of electric-field-induced coherent Raman scattering

AFOSR/AOARD Reference Number: AOARD-10-4074

AFOSR/AOARD Program Manager: Dr. Rengasamy Ponnappan

Period of Performance: April 2010 – April 2011

Submission Date: June 7, 2011

Principal Investigator:
Tsuyohito Ito, Osaka University

Report Documentation Page

Form Approved
OMB No. 0704-0188

1. REPORT DATE	2. REPORT TYPE	3. DATES COVERED
13 JUN 2011	**FInal**	**09-04-2010 to 08-04-2011**

4. TITLE AND SUBTITLE
Fundamental studies of electric-field-induced coherent Raman scattering

5a. CONTRACT NUMBER
FA23861014074

5b. GRANT NUMBER

5c. PROGRAM ELEMENT NUMBER

6. AUTHOR(S)
Tsuyohito Ito

5d. PROJECT NUMBER

5e. TASK NUMBER

5f. WORK UNIT NUMBER

7. PERFORMING ORGANIZATION NAME(S) AND ADDRESS(ES)
Osaka University,2-1-A12 Yamadaoka,Osaka 565-0871,Japan,JP,565-0871

8. PERFORMING ORGANIZATION REPORT NUMBER
N/A

9. SPONSORING/MONITORING AGENCY NAME(S) AND ADDRESS(ES)
AOARD, UNIT 45002, APO, AP, 96337-5002

10. SPONSOR/MONITOR'S ACRONYM(S)
AOARD

11. SPONSOR/MONITOR'S REPORT NUMBER(S)
AOARD-104074

12. DISTRIBUTION/AVAILABILITY STATEMENT
Approved for public release; distribution unlimited

13. SUPPLEMENTARY NOTES

14. ABSTRACT
A rather novel method has been studied, referred to here as electric-field-induced coherent Raman scattering (E-CRS). Two beams of laser pulses of frequencies, whose energy difference matches to the Raman transition, produce an infrared (IR) coherent beam corresponding to the Raman transition energy in the presence of a direct-current (dc) electric field. The IR light may be considered as an anti-Stokes wave generated by the electric fields of two laser beams and a third field at zero frequency, i.e., the dc electric field. The same laser beams also produce conventional coherent anti-Stokes Raman scattering (CARS) regardless of the presence of the dc electric field. The electric field can be extracted by the signal ratio (IR vs. CARS), which depends only on the electric field strength. This method, using nanosecond laser beams, has the potential to be a powerful tool to reveal rich high-speed dynamics in discharge plasmas.

15. SUBJECT TERMS
Propulsion, Plasma Dynamics, Raman Scattering, Electron density measurement

16. SECURITY CLASSIFICATION OF:			17. LIMITATION OF ABSTRACT	18. NUMBER OF PAGES	19a. NAME OF RESPONSIBLE PERSON
a. REPORT	b. ABSTRACT	c. THIS PAGE			
unclassified	**unclassified**	**unclassified**	**Same as Report (SAR)**	**11**	

Abstract

A rather novel method has been studied, referred to here as electric-field-induced coherent Raman scattering (E-CRS). Two beams of laser pulses of frequencies, whose energy difference matches to the Raman transition, produce an infrared (IR) coherent beam corresponding to the Raman transition energy in the presence of a direct-current (dc) electric field. The IR light may be considered as an anti-Stokes wave generated by the electric fields of two laser beams and a third field at zero frequency, i.e., the dc electric field. The same laser beams also produce conventional coherent anti-Stokes Raman scattering (CARS) regardless of the presence of the dc electric field. The electric field can be extracted by the signal ratio (IR vs. CARS), which depends only on the electric field strength. This method, using nanosecond laser beams, has the potential to be a powerful tool to reveal rich high-speed dynamics in discharge plasmas.

Such potential has been demonstrated by revealing rapid breakdown mechanisms of nanosecond-pulsed dielectric barrier discharges generated in open air. Our experimental observations have revealed that, in the pre-breakdown phase of the nanosecond DBD discharge, the externally applied fast-rising electric field is strongly enhanced near the cathode due to large accumulation of space charge, which then strongly enhances ionization near the cathode. Once a sufficiently large number of ionizations take place, the location of peak ionization forms a front and propagates toward the cathode with strong optical emission, which establishes the discharge. This process is essentially different from the well-known Townsend mechanism for slower discharges, in which ion transport to the cathode for continuous generation of secondary electrons is considered to be a prerequisite for discharge breakdown.

Objectives and contents

The ultimate targets of this study are to measure both macroscopic electric field and microscopic electric field (for estimating electron density) by E-CRS with nanosecond temporal resolutions, to reveal rich high-speed dynamics in discharge plasmas.

In the period of the funding, we have successfully revealed very high-speed discharge dynamics in high-pressure discharges with E-CRS method, while successful measurements of microscopic electric field, as well as reducing the environmental pressure, still requires further study probably with a more sensitive measurement system.

This report, based on the successful results, has components related to: (a) description of the electric field measurement method and (b) successful demonstration revealing high-speed dynamics in nanosecond-pulsed discharges.

a) Electric-field-induced coherent Raman scattering (E-CRS)

In this section, I describe the measurement method, electric-field-induced coherent Raman scattering. This method was first proposed and demonstrated by a Russian group in mid 90's [1-3] for hydrogen molecules. After that, no one else has worked on this method. Very recently, I have revisited the subject and successfully measured the electric field in hydrogen. With E-CRS method, our group has revealed very fast discharge dynamics in repetitively pulsed nanosecond discharges [4] and first demonstrated the feasibility of this method in an open air environment by using nitrogen molecules [5].

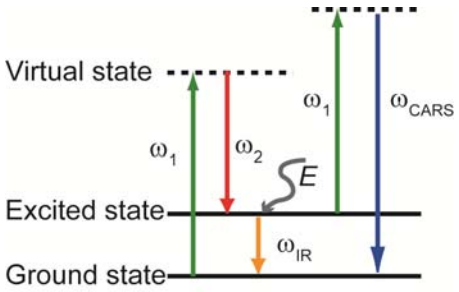

Fig. 1 Schematic energy diagram for the electric field measurement.

The schematic energy diagram of the Raman transition is shown in Fig. 1. Two beams of laser pulses of frequencies ω_1 and ω_2, whose energy difference matches to the Raman transition, produce an infrared (IR) coherent beam corresponding to the Raman transition energy in the presence of a direct-current (dc) electric field E. The IR light may be considered as an anti-Stokes wave generated by the electric fields of two laser beams and a third field at zero frequency, i.e., the dc electric field. The same laser beams also produce conventional coherent anti-Stokes Raman scattering (CARS) regardless of the presence of the dc electric field. The coherent Raman scattering beam intensities, which we denote by I_{IR} and I_{CARS}, may be written [1,5] as

$$I_{IR} = C_1 \left(N_g - N_{ex}\right)^2 I_1 I_2 E^2 \qquad (1)$$

and

$$I_{CARS} = C_2 \left(N_g - N_{ex}\right)^2 I_1^{\,2} I_2 , \qquad (2)$$

where C_1 and C_2 are constants, I_1 and I_2 the intensities of incident two laser beams of frequency ω_1 and ω_2, and N_g and N_{ex} the number densities of nitrogen molecules at the ground and excited levels involved in the transition. By eliminating the number densities from Eqs. 1 and 2, one obtains

$$E^2 = \frac{C_2}{C_1}\frac{I_1 I_{IR}}{I_{CARS}} . \qquad (3)$$

Thus the signal ratios may be considered to depend only on the electric field as

$$|E| = C_3 \sqrt{\frac{I_{IR}}{I_{CARS}}} \qquad (4)$$

with C_3 being a constant for a specific experimental setup, assuming I_1 is a constant. It has been confirmed under our experimental conditions, that C_3 is indeed almost independent of the gas parameters such as the nitrogen density or temperature in a given optical arrangement, as shown in Fig. 2 [5]. The molecular density can vary widely during a discharge or from discharge to discharge, depending on, e.g., input power, excitation frequencies, or simply the gas temperature. The fact that the proportional parameter C_3 of Eq. 4 is independent of the molecular density significantly simplifies the use of Eq. 4 for field measurement.

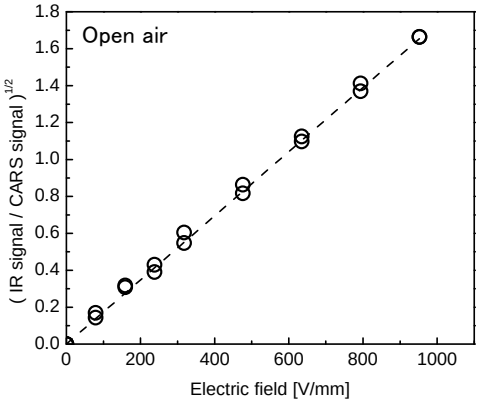

Fig. 2 Square roots of the signal ratios of IR to CARS as a function of the externally applied dc electric field in open air (1 atm and 293 K). At each electric field value given here, two independent sets of experiments were performed. Each data point represents a signal value averaged over 100 laser shots. The dashed line represents a liner fit to all data points shown here [5].

b) Electric field measurements in open-air dielectric barrier discharges

[based on the publication 1]

Atmospheric pressure plasmas (APPs) with low gas temperature, especially those made by dielectric barrier discharges (DBDs), are used in various applications, such as materials synthesis [6], environmental applications [7], biological applications [8-11], and aerodynamic controls [12]. A better understanding of the discharge mechanisms of such plasmas is expected to contribute to the development of better plasma generation systems specific for each application.

When APPs are used with low gas temperature, plasmas are typically generated as series of pulsed discharges so that the ambient gas is cooled sufficiently after each discharge pulse. Each discharge pulse can last only for a very short period (e.g., on the order of a few dozen nanoseconds) and therefore the discharge initiation process often characterizes the nature of such a discharge pulse.

However, detailed discharge characteristics in the initiation phases of APPs are far from being well understood mostly because only a few diagnostic techniques are available for the measurement of such plasmas. The discharge initiation process generally includes a pre-breakdown phase followed by

breakdown with cathode-directed ionization front propagation. The propagation creates large amounts of charges in space and increases the electrical conductivity of the plasma [13].

For a parallel plate discharge, if the electric field generated between the electrodes evolves slowly to the extent that the field may be considered to be nearly stationary (i.e., constant in time and uniform in space) with respect to electron and ion motions, an electron avalanche takes place between the electrodes initiated by with a small number of preexisting electrons when the field is sufficiently strong. According to the Townsend theory [14], if ions generated in the electron avalanche are transported to the cathode and generate sufficiently many secondary electrons there, then the electron avalanche continues or even grows in time. When this cycle of secondary electron emission by ion impact and ion generation by secondary electrons is established, "breakdown" is considered to have taken place. Prior to breakdown (i.e., in the pre-breakdown phase), the externally applied field essentially remains uniform in space and, after breakdown, the field develops its spatial variation due to accumulated space charges. This rapid evolution of the electric field typically manifests itself as cathode-directed ionization front propagation [13].

What is essential for discharge breakdown in the Townsend theory is incessant emission of secondary electrons. In other words, in Townsend theory, breakdown would not occur unless ions move across the electrode gap to generate secondary electrons [15,16].

However, if the externally applied electric field evolves far more rapidly than ions cross the electrode gap, a totally different discharge breakdown process can take place. In such a process, a discharge breakdown typically takes place before most ions in the system have enough time to reach the cathode [4]. This does not mean that secondary electrons play unimportant roles in such a discharge, but obviously a cycle of secondary electron emission by ion impact and ion generation by secondary electrons, as in Townsend theory, does not explain the discharge breakdown. If secondary electron emission of Townsend theory is not essential for breakdown, what is the breakdown mechanism?

The goal here is to answer this question by observing carefully the initiation phase of DBDs in air. The observations we made are the time evolutions of electric fields and optical emission in the gap of parallel plate discharge electrodes.

The experiments were conducted with a parallel plate DBD discharge system shown in Fig. 3. Each electrode is made of brass and circular in shape with a diameter of 6 mm. It is covered with a glass plate of 0.15 mm in thickness whose relative permittivity is about 4.6. The gap distance, defined here as the distance between the dielectric surfaces, is 0.85 mm with the accuracy of about 0.05 mm. With this configuration, the discharge is essentially one-dimensional in space. During the measurements presented in this letter, the temperature and the humidity of the environment were approximately 300 K and 50%.

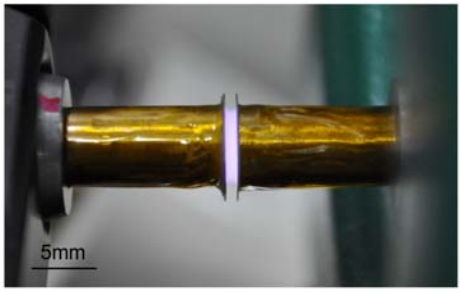

Fig. 3 Photograph of the repetitively-pulsed nanosecond dielectric barrier discharge generation.

The repetitively pulsed nanosecond voltage was applied to one of the electrodes (which will be referred to as "cathode" in this letter) by a power supply (FID GmbH: FPG20-100MC2). The other electrode is connected to the ground. The peak voltage was about -3.5 kV and its duration with discharge generation was about 15 ns in full-width of half maximum (FWHM) as shown in Fig. 4, with the repetition rate of 10 kHz. The discharge current measured with a current probe (Pearson Electronics: 6585) at the ground electrode is also shown by the broken curve in Fig. 4. The gas temperature estimated from the coherent anti-Stokes Raman scattering signal reduction throughout the experiments of this study is at most 340 K.

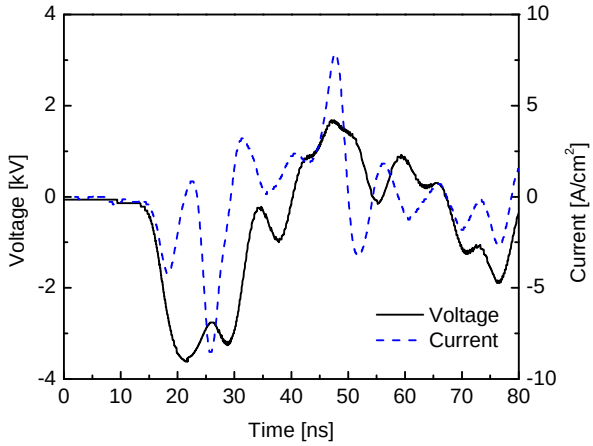

Fig. 4 Temporal evolution of the applied voltage (black line) and the current (blue broken line).

Figure 5 shows a schematic diagram of the measurement system, where two pulsed nanosecond laser beams (532 nm and 607 nm) with durations of 3-5 ns FWHM are employed. The laser energies per pulse are about 10 mJ at 532 nm and about 5 mJ at 607 nm. The repetition rate for both lasers is 10 Hz and their synchronization with discharge pulses is controlled by a delay generator (Stanford Research: SR535). The laser beams are focused on the axis of the discharge by a lens with 20 cm focal length. The size of both beam wastes is approximately 150 μm. Polarizations of the laser beams are set to be in the direction of the electric field in this study.

In atmosphere with nitrogen molecules, the two laser beams together with an electric field induce coherent infrared (IR) radiation at a wavelength of 4.29 μm, which may be considered as an anti-Stokes light of the electric field (i.e., "light" with near-zero frequency). The same laser beams also produce ordinary coherent anti-Stokes Raman scattering (CARS) radiation at 473 nm. The IR and CARS radiations are called CRS radiations. The IR and CARS signals are detected by an InSb detector and a photodiode. In evaluating Eq. 4 in the section (a), we have used data averaged over 50 measured signals. As to system calibration (for the constant C_3 in Eq. 4 and relative timing between laser and power supply), we performed time-dependent field measurement *in the absence of a discharge* as in the previous study [4], taking into account the fact that the 93% and 7% of applied voltage appear in the gap and dielectrics. Time evolution of the electric field measured at the center of the gap is shown by

open circles in Fig. 6. It is clearly seen that the measured electric field deviates from the nominal electric field value at around 19 ns, which indicates the presence of space charge.

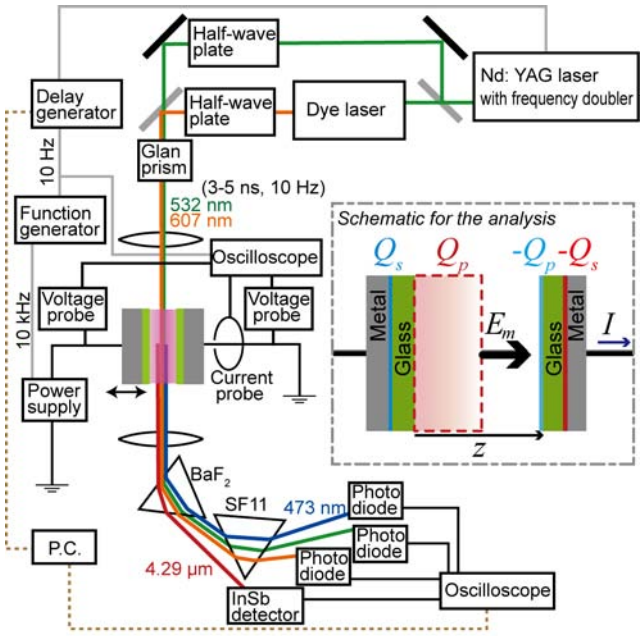

Fig. 5 A schematic diagram of the electric field measurement system. The inset is a schematic denoting symbols employed for the analysis.

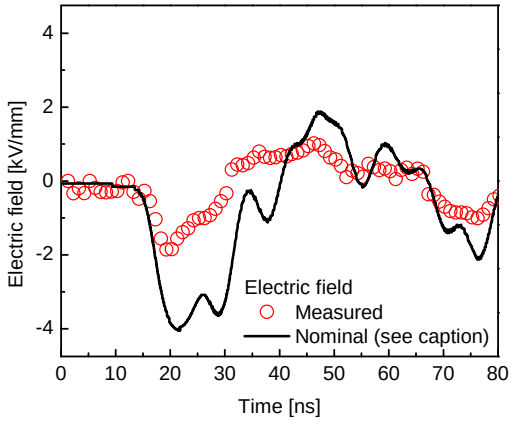

Fig. 6 Temporal evolution of the nominal electric field (the electric field expected without any space charge: solid curve), and electric field at the center of the gap measured by E-CRS (empty circle). The nominal electric field is defined here as the 93% of applied voltage divided by the gap length (The 7% of applied voltage is taken up by the dielectric barrier layers on the electrodes.)

Figure 7 shows the emission intensity as a function of the time and position measured by an Intensified Charged Coupled Device (ICCD) camera (Hamamatsu Photonics: C8484-05G01 and C7164-03). Its gate width is 250 ps and the time step is 100 ps. The images are averaged over 1000 samples. No filter was employed and therefore all the visible light from the discharge has been captured. The horizontal axis for time is essentially the same as that for Fig. 6. Synchronization of the time axis between Figs. 6 and 7 was achieved by equating the time for the lowest electric field strength of Fig.6 with the time for the weakest optical emission of Fig. 7 (at around 30.5ns). The vertical axis represents the position measured from the dielectric surface of the cathode.

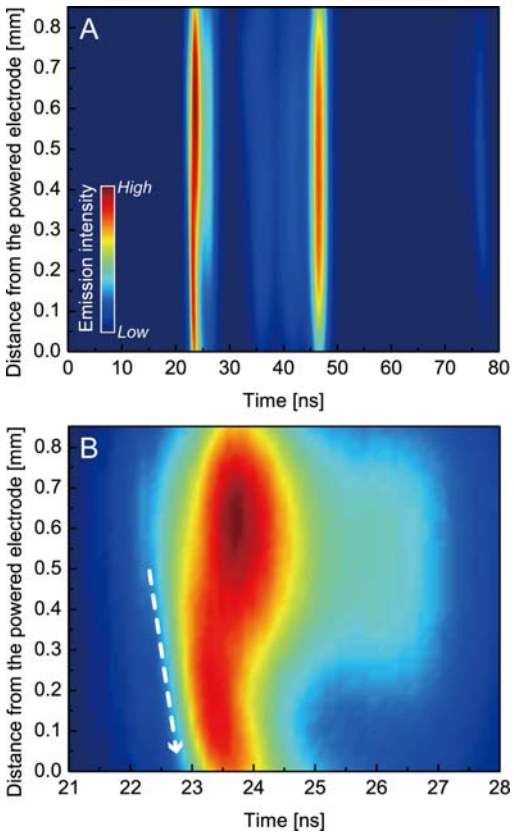

Fig. 7 Spatio-temporal distribution of the emission intensity obtained from an ICCD camera; A: 0-80 ns, B: 21-28 ns. The white dashed arrow in (B) is a guide to the eye for the emission propagation with a propagation velocity of approximately 10^6 m/s.

Figure 7 (A) shows that strong optical emissions appear at around 23 ns and 47 ns. Relatively weak emissions are also seen at around 26, 36, 41, and 76 ns. The expanded view of the emission at around 23 ns is given in (B), where an optical emission is seen to propagate from a region near the anode towards the cathode with a velocity of 10^6 m/s. It should be noted that, at 19 ns when the electric field clearly deviates from the nominal field in Fig. 6, no emission is seen in Fig. 7. This indicates

a significant space charge accumulates well before the discharge breakdown (accompanied by strong optical emission).

If we denote the electric field at the center ($z = 0.425$ mm with z being the distance from the dielectric surface of the cathode) as E_m and the charge on the cathode metal per unit area of the cathode surface as Q_s, then the space charge Q_p between $z = 0$ and $z = 0.425$ mm per unit area of the electrode surface is given by

$$Q_p = \varepsilon_0 E_m - Q_s .$$

The electrode charge Q_s is evaluated from the integration of the cathode current shown in Fig. 4. It should be noted that the charge Q_p essentially represents space charges of ions that are located in the region of $0 < z < 0.425$ mm with few ions being attached to the cathode dielectric surface as ions have little time to move toward the cathode.

Time evolution of the estimated charge Q_p in the half space near the cathode is shown in Fig. 8. For reference, emission intensities given in Fig. 7(A) are also superimposed on Fig. 8. Clear synchronization is seen between the optical emission and charge Q_p, such as strong optical emission at the inflection point of charge evolution at around 23 ns, the lowest emission near the charge maximum at around 30 ns, and another strong emission near the change in charge polarity at around 46 ns, which indirectly supports the assumption employed for time synchronization between Figs. 6 and 7 mentioned earlier.

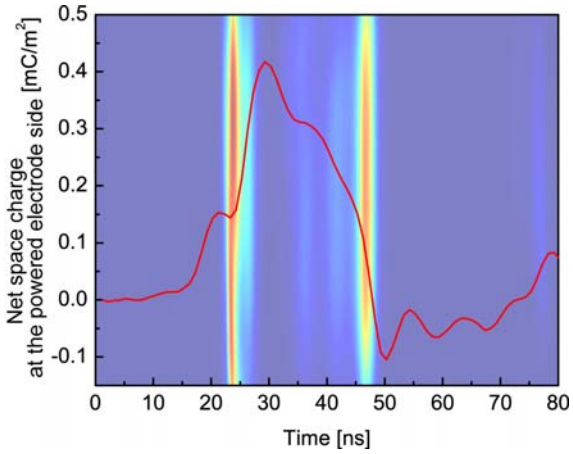

Fig. 8 The estimated charge Q_p in the half space near the cathode, evaluated from the electric field and charge on the cathode. The background is the map of optical emissions of Fig. 7 with slightly lighter color tones.

It is interesting to note that a significantly large net charge ($Q_p \approx 0.15$ mC/m^2) is already accumulated in the half space near the cathode prior to detectable optical emission (breakdown) at around 23 ns. Since the maximum charge there during the discharge is approximately 0.4 mC/m^2, as seen at around 30 ns in Fig. 8, more than one third of the maximum net charge is shown to be formed already in the pre-breakdown phase.

The positive charge shown here is likely to come from a tenuous plasma that is a remnant from the preceding discharge pulse. When a large electric field is applied, the electrons move towards the anode, leaving behind the positive ions which hardly move in the time scale considered here. While

many electrons may be attached to the dielectric surface of the anode (i.e., grounded electrode in our system), most ions stay in space. Assuming that the electron motion is mostly of electric-field drift and its velocity in the z direction is given by $v = \mu E$ with μ and E being the electron mobility and electric field. The distance d_e of electron drift between time $t = 0$ and T is then given by

$$d_e = \left| \mu \int_0^T E dt \right|,$$

which is about 0.3 mm at $T = 18$ ns with $\mu = 5.9\times10^{-2}$ m^2/Vs [14] and the integral of the electric field being -5×10^{-9} kV·mm^{-1}·s evaluated from the field values at the center given in Fig. 6. If the initial plasma is uniformly distributed, then the net positive charge Q_p at $T = 18$ ns may be given from the relation

$$Q_p = e\, d_e\, n_{i0}$$

with e and n_{i0} being the elementary charge and ion density of the initial plasma. Using the values given above and Fig. 8, we obtain

$$n_{i0} \approx 2\times10^{18}\ \text{m}^{-3}.$$

In the pre-breakdown phase, space charge developed in this phase shields the electric field. In an attempt to maintain a high voltage between the electrodes, the power supply pumps more electrons to the cathodes, resulting in a larger electric field at and near the cathode. Using Q_s obtained from the integration of current given in Fig. 4, we evaluate the electric field at the cathode from the relation $E_{cat} = Q_s/\varepsilon_0$, assuming that few ions have been adsorbed by the cathode dielectric surface as there is little time for most ions reach the surface. For example, at $t = 19$ns, the cathode charge per unit area is -0.1 mC/m^2, which means $E_{cat} \approx$ -10kV/mm, significantly larger in magnitude than the nominal electric field given in Fig. 6. This is an enhancement of the electric field near the cathode in the pre-breakdown phase due to charge accumulation.

Since the electron drift motion of pre-existing plasma (i.e., a remnant from the preceding discharge pulse) toward the anode that leaves behind nearly motionless ions is the first step for the enhancement of the electric field near the cathode, such electrons have little chance to be accelerated by the enhanced field. On the other hand, secondary electrons are the ones that are accelerated by the electric field near the cathode. Although ions hardly move in the time scale of interest, ions that are initially located very close to the cathode do reach the cathode in this time scale and generate some secondary electrons. Although the number of secondary electrons in this discharge may be small, their acceleration by the enhanced electric field and consequently their ability to ionize may not be neglected.

Since the ionization coefficient a has a strong dependence on the electric field, the enhancement of the field near the cathode contributes significantly to the enhancement of ionization in the bulk. For example, in air, the ionization coefficient a is approximately 1 cm^{-1} at an electric field of 2 kV/mm and increases exponentially with the field, reaching ~80 cm^{-1} at 4 kV/mm, ~400 cm^{-1} at 6 kV/mm, and ~10^3 cm^{-1} at 10 kV/mm [17]. Therefore, even a small number of secondary electrons emitted from the cathode can generate large space charge in the pre-breakdown phase due to the large ionization coefficient a arising from the enhanced field.

In summary, from time-resolved experimental measurements of fast initiation phases of parallel plate DBDs, we have shown that, when the externally applied field evolves much faster than the time scale for ions to move across the gap, the discharge breakdown is caused by a mechanism essentially different from Townsend theory. With a fast evolving externally applied field, a discharge breakdown takes place well before ions generated by ionization in the bulk impact the cathode and cause secondary electron emission. In the pre-breakdown phase of such a discharge, significant charge accumulation

occurs. This charge accumulation is caused by charge separation of the initial plasma remaining from the previous discharge pulse as well as ionization caused by secondary electrons accelerated by the enhanced field near the cathode. The key here is the enhancement of the electric field near the cathode in the pre-breakdown phase. The field enhancement is caused by compensating power input from the external circuit to maintain a high gap voltage when a space charge formed near the cathode strongly shields the externally applied field. Since ions have little time to move in this time scale, after electrons move toward the anode, ions remain where they were initially or at the locations where they were generated by ionization. This region of positive charge near the cathode is the very space in which an extremely large electric field is formed to sustain the discharge voltage. If the externally applied field evolved much more slowly and all ions reached the dielectric surface of the cathode, a full shielding of the electric field over the entire gap would take place and no strong field could be concentrated anywhere in the gap space.

References

[1] O. A. Evsin, E. B. Kupryanova, V. N. Ochkin, S. Y. Savinov, and S. N. Tskhai, Quant. Elect. **25**, 278 (1995).
[2] D. A. Akimov et. al., JETP Letters **70**, 375 (1999).
[3] S. N. Tskhai et. al., J. Raman Spec. **32**, 177 (2001).
[4] T. Ito, K. Kobayashi, U. Czarnetzki, and S. Hamaguchi, submitted.
[5] T. Ito, K. Kobayashi, S. Mueller, D. Luggenhölscher, U. Czarnetzki, and S. Hamaguchi, J. Phys. D: Appl. Phys. **42**, 092003 (2009).
[6] C. Nessim, M. Boulos, U. Kogelschatz, Eur. Phys. J. Appl. Phys. **47**, 22819 (2009)
[7] P Baroch, N Saito, O. Takai, J. Phys. D: Appl. Phys. **41**, 085207 (2008).
[8] G. Fridman, G. Friedman, A. Gutsol, A. B. Shekhter, V. N. Vasilets, A. Fridman, Plasma Process. Polym. **5**, 503 (2008).
[9] M. G. Kong et. al., New J. Phys. **11**, 115012 (2009).
[10] M. Laroussi, IEEE Trans. Plasma Sci. **37**, 714 (2009).
[11] T. Ito, T. Ito, S. Yokoyama, Appl. Phys. Express **4**, 026201 (2011).
[12] T. N. Jukes, K.-S. Choi, Phys. Rev. Lett. **102**, 254501 (2009).
[13] E. Wagenaars, M. D. Bowden, G. M. W. Kroesen, Phys. Rev. Lett. **98**, 075002 (2007).
[14] Y. P. Raizer "Gas Discharge Physics" Springer-Verlag (1991).
[15] T. Hoder, R. Brandenburg, R. Basner, K.-D. Weltmann, K. V. Kozlov, and H.-E. Wagner, J. Phys. D: Appl. Phys. **43**, 124009 (2010).
[16] Y. V. Yurgelenas, H.-E. Wagner, J. Phys. D: Appl. Phys. **39** 4031 (2006).
[17] S. C. Brown "Basic Data of Plasma Physics" AIP press (1993).

Appendix

A. Personnel Supported:

Associate Professor:	Tsuyohito Ito (P.I.)
Undergraduate Students:	Tatsuya Kanazawa
Collaborator:	Satoshi Hamaguchi (Professor, Osaka University)

B. Publications:

1. T. Ito, T. Kanazawa, S. Hamaguchi, "Rapid Breakdown Mechanisms of Open Air Nanosecond Dielectric Barrier Discharges," submitted to Phys. Rev. Lett.

C. Interactions:

Conference presentations

1. T. Ito "Advanced Diagnostics and Applications of High-Pressure Plasma Discharges," International Symposium at Frontier Research Base for Global Young Researchers, Osaka, Japan, Nov. 15-16, 2010.

2. T. Ito, T. Kanazawa, S. Hamaguchi, "Electric field measurements in open-air dielectric barrier discharges," submitted for the presentation at the 72nd Fall Meeting of the Japan Society of Applied Physics, Yamagata, Japan, Aug. 29 - Sep. 2, 2011.

D. Inventions:

None

E. Honors/Awards:

1. "The Commendation for Science and Technology by the Minister of Education, Culture, Sports, Science and Technology, The Young Scientists' Prize"
   Tsuyohito Ito
   "Microplasma Technology"
   April, 2011

F. Archival Documentation:

The submitted paper [1] is attached.
(The final version will be sent after the publication.)

G. Software and/or Hardware:

None